An Electric Field Detector for high-performance measurements of the electric field in the ionosphere

The 34th International Cosmic Ray Conference, 30 July- 6 August, 2015 - The Hague, The Netherlands

D. Badoni * [ab], G. Masciantonio [ac], P. Cipollone [b], G. Vannaroni [de], P. Diego [cd], R. Ammendola [b], V.A. Belyaev [f], O. Simonelli [g] for CSES-LIMADOU Collaboration

[a] Department of Physics, University of Rome Tor Vergata, Via della Ricerca Scientifica 1, I-00133 Rome, Italy; [b] INFN, Sez. of Rome Tor Vergata, Via della Ricerca Scientifica 1, I-00133 Rome, Italy; [c] Department of Physics, University of Trento, 38123 Povo (TN), Italy; [d] INAF/IAPS, Roma Via Fosso del Cavaliere 100, I-00133 Rome, Italy; [e] Università Telematica Internazionale Uninettuno, Corso Vittorio Emanuele II 39, 00186 Rome, Italy; [f] National Research Nuclear University MEPhI, Moscow, Russia; [g] Innovation Design S.r.l., Via Libero Leonardi 4, 00173 Rome, Italy.

* davide.badoni@roma2.infn.it

1 Introduction

We have designed and realized a new electric field detector (EFD) to be installed on board scientific space missions suitable to investigate electromagnetic phenomena in ionosphere. The instrument measures electric field in a large bandwidth from quasi-DC up to about 5 MHz. The resolution of the proposed instrument in the ULF band is better than $1\mu V/m$ with a dynamic range of $120\ dB$. The sensitivities in the other bands (ELF, VLF and HF) are better than $300\,\frac{nV}{\sqrt{Hz}}$. Considering the boom lengths, it can be expressed in terms of electric field and becomes of the order of $50\,\frac{nV}{\sqrt{Hz}\,m}$. We present the description of the instrument electronics and the results of the preliminary tests performed on the EFD prototype in laboratory. The general EFD block diagram is shown in fig. 1.

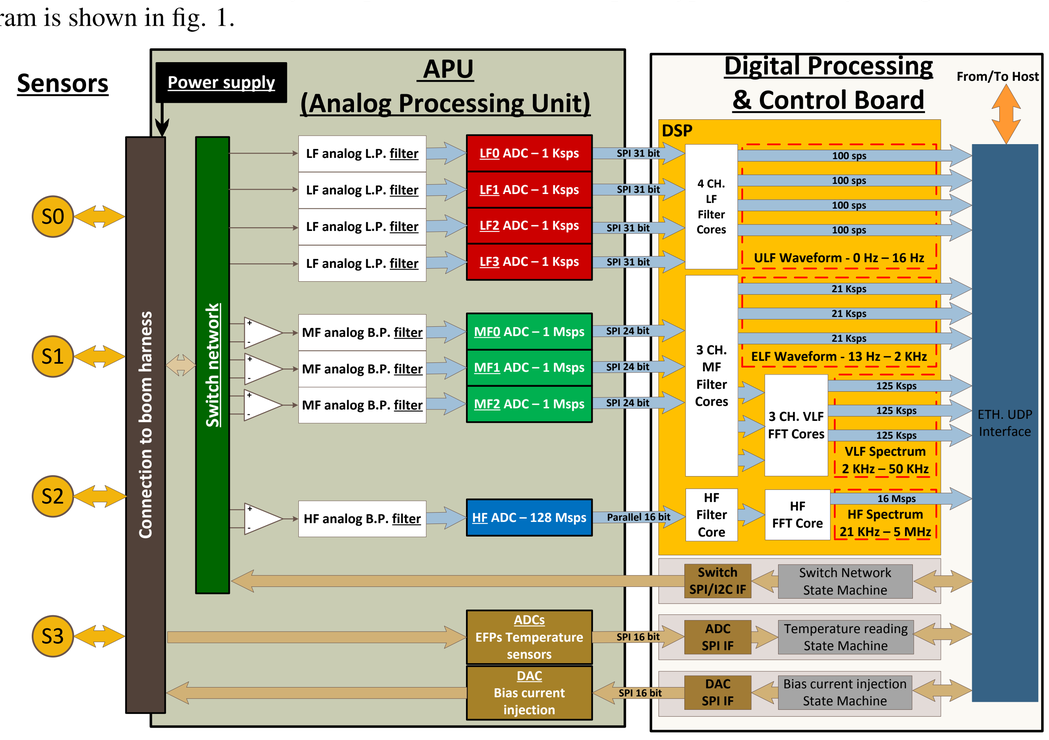

Figure 1: EFD block diagram.

The instrument consists of four independent identical sensors (from $S0$ through $S3$) followed by two boards for signal conditioning, digital conversion and processing. The sensors are installed at the tips of four booms (about four meters long) deployed from a 3-axes stabilized spacecraft. The Analog Processing Unit (*APU*) performs a fully flexible selection of the sensors and provides a preliminary filtering and band subdivision. The Digital Processing & Control Board carries out a decimation process for ULF and ELF bands, the Fast Fourier Transform for VLF and HF bands and transmission control of data & commands to/from host PC and APU.

2 Description

Description of the sensors

The electric field will be derived by dividing the potential difference measured across a pairs of sensors to their mutual distance.

Each sensor consists of a spherical electrode exposed to the ionospheric plasma connected to a very high input impedance voltage follower. The block diagram of one EFD sensor is shown in fig. 2 along with photograps of the prototype.

The contact impedance (dV/dI) between electrode and plasma reaches a minimum when the electrode is biased at the plasma potential (assumed equal to zero) whereas significantly increases when the electrode acquires a negative potential. Usually a floating electrode in plasma acquires a negative potential (floating potential), thus the EFD has to use a current generator in order to bias itself close to the plasma potential to minimize the contact impedance and improve the measurement accuracy.

The electronics is shielded from the external current collecting electrode through an inner conductive shell which is bootstrapped at sensor potential in order to minimize the effect of the stray capacitance. The short stubs placed at the opposite sides of the EFD (aligned with the boom axis) aim at reducing the asymmetry introduced by the presence of the boom and are bootstrapped at the same potential of the sensor. The low-pass filter visible in fig. 2 is used to optimize the frequency response of the amplifier.

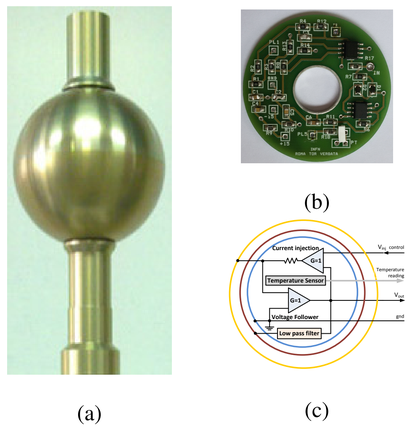

Figure 2: EFD probe prototype. Photograph of sensor (a) and board(b). (c) Block diagram: orange line represents the sensor current collector, brown is the inner bootstrapped shield and blue is the grounded shield.

Description of the Analog Processing Unit (APU) and Digital Processing & Control Board (DPCB)

The architecture of the APU is depicted in fig. 1. Its main purpose is subdivide the signals coming from the sensors into three bands: LF from 0 to $16\,Hz$; MF from $13\,Hz$ to $50\,kHz$ and HF from $21\,kHz$ to $5\,MHz$. We have four single channels for the LF band, the output signals are digitized with 31 bit ADC at $1\,ksps$ data rate.

APU Name	APU Freq. range	DPCB Name	DPCB Freq. range	OUTPUT
LF	$0-16\,Hz$	ULF	$0-16\,Hz$	Waveform
MF	$13\,Hz-50\,kHz$	ELF	$13\,Hz-2\,kHz$	Waveform
		VLF	$1\,kHz-50\,kHz$	Spectrum
HF	$21\,kHz-5\,MHz$	HF	$21\,kHz-5\,MHz$	Spectrum

Table 1: Definition of the frequencies bands.

For the MF band there are three independent channels, the output signal are sampled with 24 bit $ADCs$ at $1\,Msps$ data rate. There is a unique channel for the HF band whose signal output is sampled with 16 bit $ADCs$ at $128\,Msps$ data rate. The input of the MF and HF channels can be connected to the sensor through a switch matrix allowing a complete flexible reconfigurability. The APU contains the DAC needed to command the suitable bias current for the sensors.

The *DPCB*, described in fig. 1, provides a further digital elaboration on the APU output data (DSP block) in order to: i) improve the filter roll-off, ii) separate the MF bands into ELF and VLF bands, iii) built the FFT spectra of the VLF and HF bands. See table 1 for details. Moreover the $DPCB$ implements the digital stimuli for the bias current and the ethernet protocols for connection and data exchange to a host computer.

3 Test results

Due to the high input impedance of the sensors, a Faraday cage has been used to shield the sensors in order to protect them from external electromagnetic noise.

All measurements were carried out taking the signals from the outputs of each analog processing chain (just at the ADCs inputs) prior digitization.

We have performed the tests varying two parameters: i) the equivalent electric circuit which represents the *plasma coupling impedance* and ii) the bias current.

Values of the plasma impedance are estimated for three different combinations of plasma densities and temperatures which can be considered as the extremes and medium values expected along the CSES orbit. The plasma coupling parameters adopted for measurements are shown in table 2. These represent the extreme and typical values of possible plasma conditions encountered along a ionospheric orbit [2].

	Plasma conditions Density	Temperature	Impedance Res.	Cap.
C_1:	$10^{12}\ m^{-3}$	$3000\ K$	$67\ k\Omega$	$29\ pF$
C_2:	$10^{10}\ m^{-3}$	$2000\ K$	$660\ k\Omega$	$6.6\ pF$
C_3:	$10^{9}\ m^{-3}$	$1000\ K$	$970\ k\Omega$	$4.8\ pF$

Table 2: Plasma conditions in a ionospheric orbit and corresponding equivalent impedance values adopted.

Electronic Noise The *Electronic noise* measurements are given in terms of *Voltage Noise Spectral Density* vs frequency and determine the EFD *sensitivities* in each band. For the *LF* band the noise is given in terms of V_{rms} according to: $V_{rms} = \sqrt{\int_0^{f_{high}} (V_D(f))^2\,df}$ $(eq.\ 1)$ where $V_D(f)$ is the voltage noise density expressed in $\frac{V}{\sqrt{Hz}}$ and f_{high} is the high cutoff frequency of the LF band. The resulting V_{rms} represents the EFD resolution in that band.

Dynamic Range We define the *Dynamic range* as $DR = 20 \cdot \log \frac{V_{RMS_{MAX}}}{V_{RMS_{MIN}}}$, where $V_{RMS_{MAX}}$ is the maximum V_{RMS} obtainable at the output, in absence of distortions or saturations, whereas $V_{RMS_{MIN}}$ is the noise level.

3.1 Noise test results

Fig. 3 shows the voltage noise spectral densities for the LF, MF and HF channels measured in various plasma conditions. Panel (a) and (b) show the LF noise density for C_2 and C_3 plasma conditions, respectively. Panel (c) gives the noise measured for MF band under C_2 plasma condition. Panel (d) provides the noise measured for HF band for C_2 plasma condition.

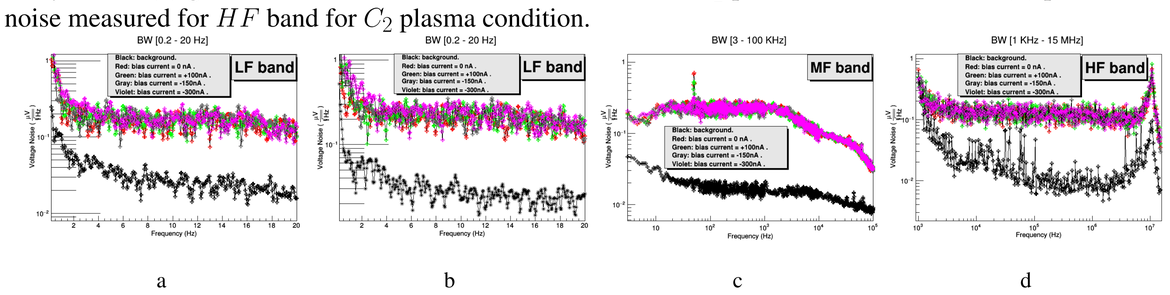

a b c d

Figure 3: Voltage noise spectral density vs frequency: (a) *LF* channel with for C_2 plasma condition; (b) *LF* channel for C_3 plasma condition; (c) *MF* channel for C_2 plasma condition; (d) *HF* channel for C_2 plasma condition. All tests have been obtained for several values of the *bias current*. The black traces represent the noise due to the measurement instrumentation determined while the EFD electronics is powered off.

Table 3 shows the results of the calculated V_{rms} noise for various bias currents obtained with different plasma conditions applying eq. (1).

The results show that the noise spectral density is almost independent from the values of the injected bias current. On the basis of the CSES configuration, which foresees boom lengths of about four meters (about eight meters tip to tip), the electric field resolution is better than $1\mu V/m$.

Configuration	Plasma condition C_1	C_2	C_3
Bias current $= 0\,nA$	$0.60\,\mu V_{rms}$	$0.96\,\mu V_{rms}$	$1.14\,\mu V_{rms}$
Bias current $= 100\,nA$	$0.65\,\mu V_{rms}$	$1.16\,\mu V_{rms}$	$1.30\,\mu V_{rms}$
Bias current $= -150\,nA$	$0.72\,\mu V_{rms}$	$1.21\,\mu V_{rms}$	$1.42\,\mu V_{rms}$
Bias current $= -300\,nA$	$0.58\,\mu V_{rms}$	$1.59\,\mu V_{rms}$	$1.66\,\mu V_{rms}$

Table 3: V_{rms} noise for $LFband$ obtained by applying the eq. (1).

3.2 Dynamic range test results

We obtain the values shown in table 4.

Band	Analog chain	ADC
LF	**120** dB	$124\ dB$
ELF	**139** dB	105 dB
VLF	**115** dB	105 dB
HF	**87** dB	78 dB

Table 4: EFD: Dynamic range for each band.

We obtain $120\,dB$ for the LF band, $139\,dB$ for ELF, $115\,dB$ for VLF and $87\,dB$ for HF. Along with these data we have also shown the dynamic ranges quoted from manufacturer data-sheets of the various ADCs used for the different bands. In several bands, the dynamic ranges of ADC are worse than the ones computed for the analog chains. In those cases the actual dynamic range of the overall system is limited by the ADC performance.

3.3 Transfer function test results

Fig. 4 shows the analog transfer functions for LF (panel (a)), MF (panel (b)) and HF (panel (c)). Note that the slight decay of the transfer function amplitudes within the bandwidth of the MF and HF filters, starting at about $20\ kHz$, are due to the low-pass pole associated to the plasma coupling equivalent electric circuit used to simulate the various plasma conditions.

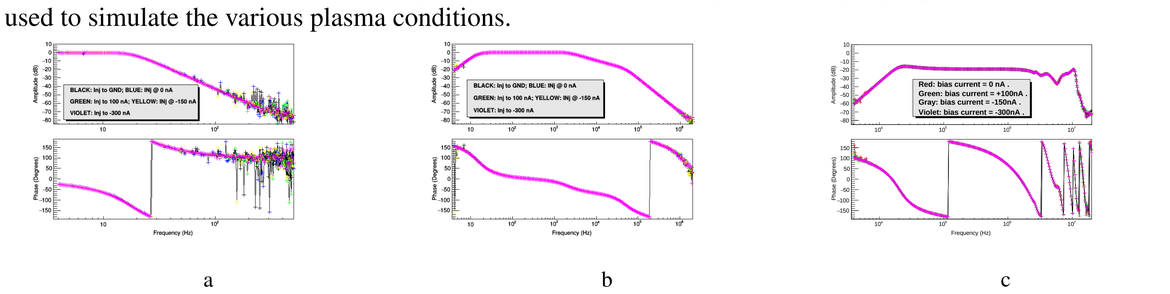

a b c

Figure 4: EFD transfer functions measured for the LF (panel a), MF (panel b) and HF (panel c) bands applying at the input the equivalent electric circuit simulating C_2 plasma condition.

Acknowledgments

This work is financially supported by the Italian Space Agency (ASI) in the frame of the "Progetto Premiale Limadou".

The authors want to thanks the Chinese collegues from Lanzhou Institute of Physics (LIP China) who partecipate to the definition of the EFD Project and in particular Ma Mianjun, Lei Jungang and Cui Yang.

References

[1] J.J. Berthelier et al., *ICE, the electric field experiment on DEMETER*, *Planet Space Sci., 54 pp.456-471, 2006.*

[2] G. Vannaroni, *Considerations on design of the front-end electronics, private comunication - May 6^{th} - 2011 giuliano.vannaroni@iaps.inaf.it* .

[3] A.V. Oppenheim, R.W. Shafer, *Digital signal processing* Prentice Hall, (1975).

[4] L.P. Huelsman, *Active and passive Analog Filter Design* Paperback, International Edition (1993).